Comparative Study on NACA-9405, NACA-9503 and NACA-9506 Airfoil Profiled Blade Open-Channel Flow Cross-Flow Turbine

Aji Putro Prakoso[1], Wirawan Piseno[2], Damawidjaya Bisono[3], Deny Bayu Saefudin[4], Ahmad Fudholi[5], Fikri Nur Rohman[6]

[1,2,3,4,6]Mechanical Engineering, Faculty of Manufacturing Technology,
Universitas Jenderal Achmad Yani (UNJANI), Indonesia
[5]Research Center for Energy Conversion and Conservation,
National Research and Innovation Agency (BRIN), Indonesia
[5]Solar Energy Research Institute, Universiti Kebangsaan Malaysia, Malaysia

E-Mail: [1]aji.putro@lecture.unjani.ac.id, [2]wirawan.piseno@gmail.com, [3]damawidjaya@lecture.unjani.ac.id, [4]denybayuunjani@gmail.com, [5]ahmad.fudholi@brin.go.id, [6]fikrinurr28@gmail.com

Abstract

Several agricultural areas in Indonesia are classified as underdeveloped rural areas, and challenging to acquire electricity from the primary grid. On the other hand, some pico hydropower potentials can be found in agriculture, especially at the irrigation dam spillway flows. However, no such technology can convert the energy inside the water open-channel flow through dam spillways into electricity. Crossflow turbines (CFT) are expected to utilize dam spillways' power due to their ability to convert the kinetic energy of water. Prior studies found that airfoil profile could slightly increase CFT efficiency and affect the interaction between water and turbine. Using planar two-dimensional computational fluid dynamics (CFD) numerical simulation analysis, the current study investigated the energy conversion phenomenon inside different open-channel CFT blade profiles. This study simulates CFT working at 3 meters of total head and 0.04 m3/s of water discharge put into the dam spillway's downstream. The turbine blade profiled with the National Advisory Committee of Aeronautics (NACA) standard airfoil numbered 9405, 9503, and 9506 are being compared and investigated in the present study. CFD numerical analysis results show that the forward direction NACA airfoil profiled blades deliver better efficiency than the reversed one. These findings contradict the prior study's results which tested airfoil profiled CFT working as usual with nozzle. This phenomenon indicated differences in the energy transfer process between open channel CFT and the ordinary CFT with a nozzle. Furthermore, current work finds that forward NACA-9503 CFT has a higher efficiency than other tested airfoil profiles, with 57.05% efficiency. In addition, the present study finds that the NACA-95XX airfoil has a more suitable chamber curve with the original CFT blade's curve than the NACA-94XX airfoil by velocity triangle analysis. Then, the NACA-9503 profile is thinner than the NACA-9506 profile, which eases water flowing through the turbine blades.

Keywords: Airfoil, Computational Fluid Dynamics (CFD), Crossflow Turbine, Hydropower Turbine, Open Channel Flow

1. INTRODUCTION

Based on Indonesia's Center of Statistics (BPS), there are still more than 13,000 villages in Indonesia classified as underdeveloped rural areas in 2018 [1]. Most of those villages depend on their economy in agriculture [2]. There is some irrigation grid inside those villages for the need of the agricultural area [3]. The irrigation grid is filled with water from one or more small dams [4]. The water level difference between the upstream and the downstream irrigation dam creates potential energy [5]. This energy could be classified as pico hydro potential as the tiniest hydropower scale.

On the other hand, some underdeveloped rural areas are still not covered by on-grid electricity for some reasons [6]. The off-grid electricity scheme is one of the proven answers to the electricity problem in isolated-underdeveloped areas [7]. Utilizing pico hydro potential on irrigation dams as a pico hydropower can be a suitable solution for isolated, underdeveloped agricultural regions. Unfortunately, no hydropower turbines work for utilizing kinetic energy inside high-velocity open channel flow (OCF) like in the dam's spillway. Undershot waterwheel, which works on medium-velocity OCF, still uses the potential power of water by damming up the flow[8], [9].

As an impulse turbine, a crossflow turbine (CFT) can theoretically utilize high kinetic energy water flow [10]. Moreover, CFT has a higher specific speed than other impulse turbines among all impulse hydro

turbines [11]. That means CFT uses more water discharge and needs a lower hydraulic head than other impulse turbines [12]. That working condition is suitable with the characteristic of OCF at the irrigation dam's spillway, which usually has not more than seven meters tall [13]. This fact supports the hypothesis that CFT has an excellent compromise to utilize kinetic energy in the spillway OCF discharge.

In the final project research, Arvian et al. [14] tried to simulate the CFT placed downstream of the spillway OCF to harvest its kinetic energy using CFD simulations. These tests were resulting that the CFT could utilize about 86% of water kinetic energy at the spillway. On the other hand, Budiarso et al. [7] found that the reversed NACA-6712 profile applied on the CFT blade could increase this turbine's efficiency. That result made Adanta et al. [15] try other shapes of NACA airfoil and found that NACA-6509 has a better performance to be applied on CFT. This study, moreover, attempts to apply NACA profiled blades using prior studies' approach to the spillway OCF CFT in Arvian et al. study.

2. MATERIALS AND METHODS
2.1 Crossflow Turbine Theory

In 2013 Sammartano et al. conducted research on crossflow turbines, then continued further research in 2016 to produce optimal results using several crossflow turbine parameters, as shown in Table 1.

Table 1. Crossflow turbine parameters

Parameter	Value	Symbol
Impeller outer diameter	160 mm	D_1
Impeller inner diameter	104 mm	D_2
Number of blades	35	N_b
Angle of attack	22°	α

In a crossflow turbine, to find out the efficiency using equations 1 to 3

$$P_T = \tau\omega = \tau\frac{2\pi n}{60} \tag{1}$$

$$P_H = \rho gQH = \dot{m}gH \tag{2}$$

$$\eta = \frac{P_T}{P_H} \tag{3}$$

Where efficiency is obtained from equation 3, where P_T is the turbine output power (watts) obtained from equation 1, where τ is torque (Nm), ω is the blade speed (rad/s), n is the number of revolutions (rpm). Meanwhile for P_H is the hydraulic power (watts) obtained from equation 2, where ρ is the density of water (kg/m^3), g is the acceleration due to gravity (m/s^2), Q is the water discharge (m^3/s), H is the head (m), and m˙ is the mass flow rate (kg/s) obtained from multiplying the density of water by the water discharge.

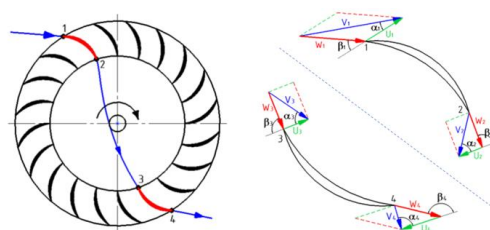### 2.2 Velocity Triangle Theory

Figure 1. Banki crossflow water turbine's speed triangle

The velocity triangle studies the basic kinematics of the water flow when it hits the water turbine blades. Based on Figure 1. The velocity triangle has several known notations that v is the absolute speed of the water, U is the tangential speed of the turbine, W is the relative speed, a is the angle of inlet water or the angle between the absolute velocity of the water (v) and the tangential velocity of the turbine (U), and the last β is defined as the angle of the blade or the angle between the relative speed (W) and the tangential speed of the turbine (U). So there are notations 1 and 2, with each note stating points for the inlet and outlet sections of the blade at the top of the turbine. Then there are also notations 3 and 4, with each notation stating points for the entry and exit

sections of the blade at the bottom turbine so that when the turbine rotates, point 1 will reach point 4 and point 2 will reach point 3; therefore it can be seen that [16]:

$$\text{Absolute speed of water} \quad : \quad V_2 = V_3 \tag{4}$$

$$\text{Circular speed} \quad : \quad U_1 = U_4 \;;\; U_2 = U_3 \tag{5}$$

$$\text{Relative speed} \quad : \quad W_1 = W_2 \;;\; W_3 = W_4 \tag{6}$$

$$\text{Blade angle} \quad : \quad \beta_1 + \beta_4 = \beta_2 + \beta_3 = 180° \tag{7}$$

The absolute speed of air entering the turbine can be calculated using the equation between the head and the velocity coefficient of the Crossflow turbine, as in equation 8 below.

$$V = \sqrt{2gH} \tag{8}$$

After obtaining V, determine the tangential velocity of water (V_T) in the Crossflow turbine using equation 9 [17].

$$V_T = V \cos(\alpha) \tag{9}$$

The turbine's efficiency can be calculated based on the speed triangle method using equation 10.

$$\eta = \frac{U_1 \, V_{T_1} - \, U_4 \, V_{T_4}}{g \; H} \tag{10}$$

2.3 Open Channel Flow Theory
In open flow, an energy equation is commonly used, this equation is the same as the Bernoulli equation, but several parameters are only found in open flow, so there are some changes to the usual Bernoulli equation. The energy equation for canal flow is stated in equation 11 [5].

$$z_1 + y_1 + \frac{v_1{}^2}{2g} = z_2 + y_2 + \frac{v_2{}^2}{2g} \tag{11}$$

Where z is the height, y is the depth or depth, and v is the velocity on the open channel, while notation one is the initial point condition and two is the notation for the endpoint.

2.4 Placement of the Airfoil Concept on the Turbine
The airfoil geometry that will be applied to the Banki crossflow water turbine must be adjusted so that the trailing edge is placed facing 90° to the tangential velocity of the turbine. But for this, the trailing edge angle of the airfoil must be known in advance using equations 12 and 13 so that later the airfoil chord can be placed correctly on the turbine.

$$\frac{d_y}{d_x} = \frac{2 \, M}{(1 - P)^2} \, (P - 1) \tag{12}$$

$$\theta_T = \tan^{-1}\left(\frac{d_y}{d_x}\right) \tag{13}$$

Where d_y/d_x is the gradient of the chamber line, M is the maximum chamber slope at 100% of the chord or divided by 100, P is the maximum chamber position at 10% of the chord or divided by 10, and θ_T is the trailing edge angle. After that, the angle chord can be obtained using equation 14.

$$\theta_C = 90° - \sin^{-1}(\theta_T) \tag{14}$$

Then a scheme for placing the airfoil concept on the Banki crossflow water turbine blades is produced, as shown in Figure 2.
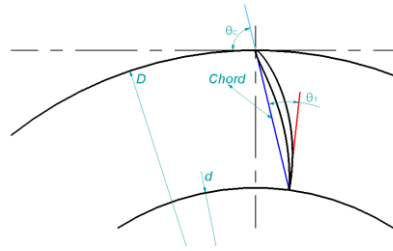
Figure 2. Schematic of crossflow water turbine blades with airfoil concept

2.5 CFD procedure
1. Pre-processing

Pre-processing is the initial stage that must be carried out before the simulation process, such as preparing the model to be simulated, meshing stages, determining condition limits, determining condition boundary values, and controlling fluid properties. In this study, the meshing steps used a quadrilateral mesh type because this type of mesh can be structured in an orderly and orderly manner, making it easier to read the mesh connectivity, and it is hoped that structured mesh will dominate. Therefore, in addition to the mesh type, the mesh size is released with two stages of mesh verification, including verification of skewness quality which aims to check the slope directly related to checking the structured mesh where the slope is the main factor to determine the quality of the structured mesh, as for the quality of the skewness mesh that must be met, as shown in Figure 3. Then, to adjust the value of the skewness quality, the mesh settings, especially in sizing, should be changed.

Figure 3. Standardization of skewness mesh quality measures

Further verification of grid independence To carry out the grid independence stages, the simulation process must be carried out several times with different mesh sizes starting from the largest to the smallest. After obtaining the simulation results, compare them with the previous results of each simulation. At the grid independence stage, there is the grid convergence index (GCI) method which is commonly used to solve grid independence using equations 15 to 18. [18]

This method finds convergent points by simulating three times using different mesh sizes but the same mesh reduction ratio. Meanwhile, to determine this ratio using equation 15 below.

$$R = \sqrt{\frac{earlier\ number\ of\ elements}{newer\ number\ of\ elements}} \tag{15}$$

While the convergence point is sought by the following equation 16.

$$f_{h=0} = f_1 + \frac{(f_1 + f_2)}{R^p - 1} \tag{16}$$

Where f is the discrete solution, and h is the grid spacing so that $f_{h=0}$ is the continuum value at zero grid spacing. The p-value is calculated using the following equation 17.

$$p = \frac{ln\left(\frac{f_3 - f_2}{f_2 - f_1}\right)}{ln\ R} \tag{17}$$

The GCI value must be below 1% [6]. GCI is calculated by the following equation 18:

$$GCI_{AB} = \frac{\frac{f_a - f_b}{f_b}}{R^p - 1} x100\% \tag{18}$$

Where f_a is the result of calculating the convergent point while f_b is the result of a simulation of the mesh point that has been used, mesh independence using GCI is done by varying the number of mesh elements with almost the same ratio and then using equation 18 to determine the GCI value; this value must be close to 1% but still below it can be used for the simulation process. as for the results of the calculation of the independence mesh.

Table 2. GCI Calculation Results

Test	Element	Ratio	Torque	Convergent Order (p)	f(h-=0)	GCI
1	14069	1,4	148,511	-2,5		4,61 %
2	27927	1,4	145,487	-2,5	133.98	1,97 %
3	55355	1,4	134,622	-2,5	133.98	0,84 %
4	108587	1,4	134,085	-2,5		0,14 %

Based on Table 2, there are two data for the number of elements that meet the requirements for a GCI value of <1%, namely the number of elements 55355 and 108587. In this study, the element value will be 55355 because the simulation is more efficient regarding time and memory on the computer, so the mesh results are presented in Figure 4 (a).

In addition to the mesh verification process, boundary conditions are identified using data that is already known or can be assumed to be the location of specific parts and the magnitude of the value. The results of the identification of boundary conditions in this study are presented in Figure 4 (b).
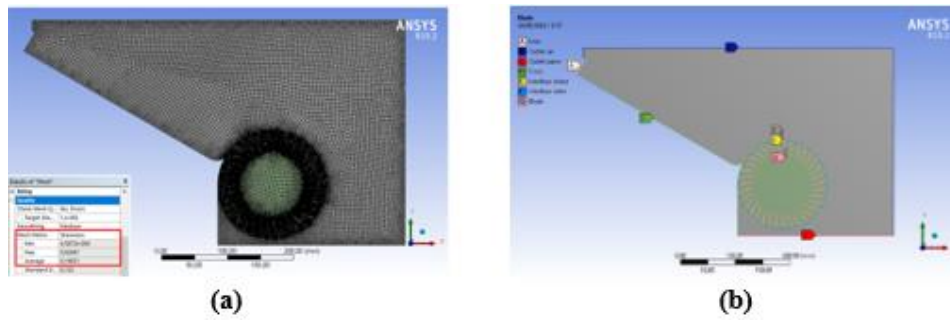

(a) **(b)**

Figure 4. (a) Mesh results; (b) Identification Boundary conditions
Based on Figure 4 (b), these boundary conditions have different types, as shown in Table 3.

Table 3 Boundary condition parameters

ID	Category	Type
A	Inlet	Velocity inlet
B	Outlet air	Pressure outlet
C	Outlet water	Pressure outlet
D	Channel	Wall
E	Interface stator	Interface
F	Interface rotor	Interface
G	Blade	Wall

2. Processing
Processing is the main stage in the simulation by calculating the conditions applied to the Pre-processing stage. This simulation uses the transient method, which uses a time-step basis. For example, with a time step size of 0.0005 s, the number of time steps or time steps used is 500, so the resulting observation time is 0.25 s, and the maximum iteration is 150 iterations. The Courant Number method is needed by using equation 19 with the Courant number value being less than one to ensure that no grid in the mesh is skipped during the simulation process to produce a good quality simulation.

$$Cr = \frac{v_s.\Delta t}{\Delta x} \tag{19}$$

$$\Delta_x = \sqrt{\left(\frac{Area}{Number\ of\ Elements}\right)} \tag{20}$$

$$v_s = \frac{L_1.E_1}{L_1 + L_2} + \frac{L_2.E_2}{L_1 + L_2} \tag{21}$$

Where the value of v_s is the average speed in the simulation, Δt is the time-step used in the simulation and Δx is the average distance of each grid, L is the area, E is the number of elements, and there is notation 1 denotes stator, and 2 denotes rotor. The parameters from the simulation results are presented in Table 4.

Table 4. Courant number calculation parameters

Section	Area (m^2)	Velocity (m/s)	Element	Area / Element
Stator	0,1139	5,88	10723	$1,06 \times 10^{-5}$
Rotor	0,0191	3,07	44632	$4,28 \times 10^{-7}$

The calculations using payments 19 to 21 show that the resulting Cr is 0.823. The result means it meets the standard, which must be less than one.

3. Post-processing

Post-processing is the data collection stage, which is the completion of the simulation with convergent simulation results. This stage uses CFD post with saved time step data and selects the 500.cdat file or the last time step of the simulation. The data obtained are contours and graphs, which can later be exported into Excel data.

3. RESULTS AND ANALYSIS
3.1 CFD Simulation
After the simulation, get some data such as torque, mass flow rate, and volume fraction of contour water. Some of these data are then entered into data processing so that the efficiency of turbine power can be known, and some other data with variations in the application of airfoils on turbine blades.

3.1.1 Torque turbine
Based on the simulations that have been carried out on the Banki crossflow water turbine, with variations in the shape of the blades, the airfoil concept shows that the differences in the shape of the blades and variations in the rotational speed of the turbine affect the torque produced, as shown in Figure 5 which is generated from the table of data from the simulation results.
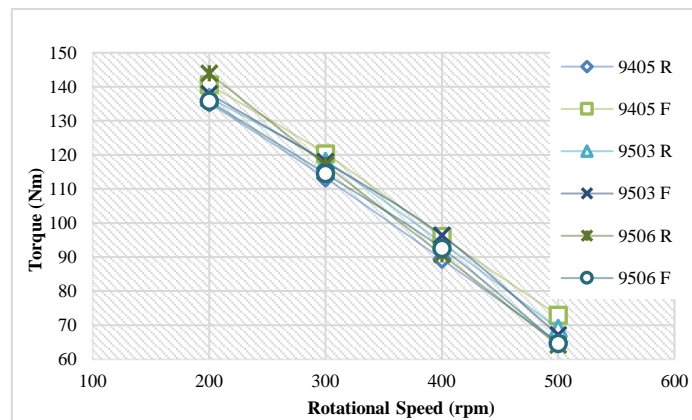

Figure 5 Graph of torque to turbine rotation speed

Based on Figure 5 shows the relationship between the turbine torque value and the turbine speed value obtained at each variation of the airfoil blade. Based on the graph, which shows that the greater the rotational speed of the turbine produced, the smaller the value of the torque generated. This condition is because when the incoming airflow with loading occurs on the turbine runner, the turbine's rotational speed slows down and increases the force resistance; this force resistance affects the value of the turbine torque produced. It was found that the highest torque value was obtained at 200 rpm, with the NACA-9506 reverse airfoil type of 143.98 Nm, while the lowest torque was at 500 rpm, with the NACA-9506 reverse airfoil of 64.19 Nm.

3.1.2 Power turbine
Furthermore, from the torque results, turbine power data is obtained using Equation 1. Finally, the data processing results are presented in Figure 6, obtained from the turbine power calculation results table.
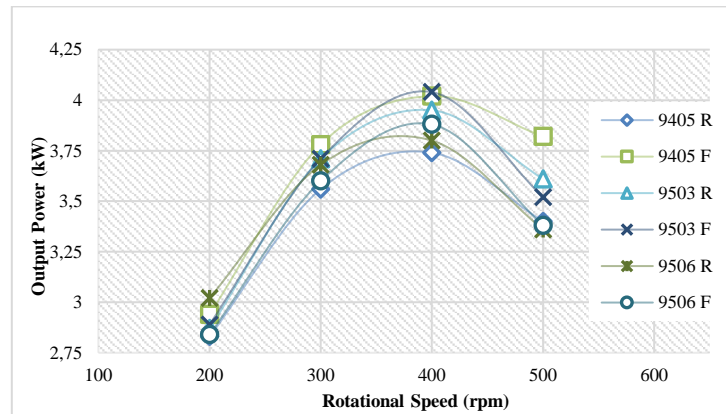
Figure 6. Graph of power to turbine rotational speed

It is based on Figure 6, which shows the relationship between the resulting turbine power and the turbine's rotational speed, which is obtained from each variation in the shape of the airfoil blade. The power value of the turbine is very dependent on the torque generated. It is known that the highest turbine power value in this study was obtained at a rotational speed of 400 rpm, with the NACA-9503 F airfoil type with a total turbine power of 4.04 kW, while the smallest turbine power value occurred at a rotational speed of 200 rpm, with the NACA type -9405 R Produces a turbine power of 2.83 kW. And it can be seen that the most undersized power for all variations is found at 200 rpm turbine rotation, while the most significant power is generated at 400 rpm turbine rotation.

3.1.3 Turbine efficiency

Then, from the results of the obtained power, it is processed, and turbine efficiency data is obtained using equation 3. Finally, the processing results for each variation of the airfoil blade are presented as shown in Figure 7, which is obtained from the turbine efficiency calculation results table.
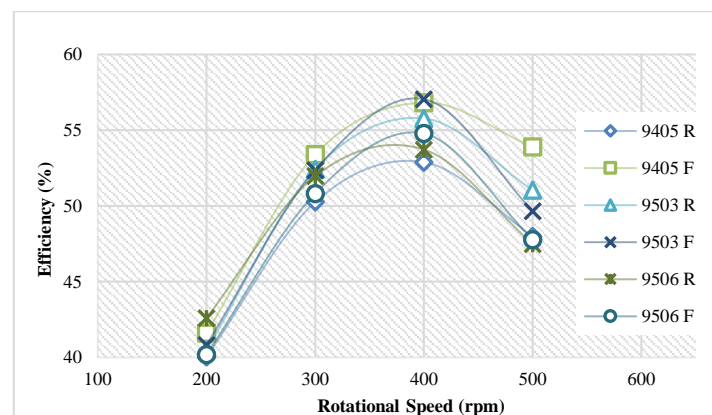

Figure 7. Graph of efficiency to turbine rotational speed

Figure 7 shows the relationship between the resulting turbine efficiency and the turbine's rotational speed, which is obtained from each variation of the shape of the airfoil blade. The value of the turbine power depends on the torque and hydraulic power value. The data processing results can be obtained for the NACA-9405 R airfoil blade variation to get the highest efficiency of 52.89%, then for NACA-9405 F to obtain the highest efficiency of 56.82%, then NACA-9503 R obtained the highest efficiency of 55.78%. At the same time, NACA-9503 F brought the highest efficiency of 57.05%, and then NACA-9506 R brought the highest efficiency of 53.72%. The last for NACA-9506 F obtains the highest efficiency of 54.78%, and it can be obtained that the highest efficiency of the turbine is found in the variation of the NACA-9503 F airfoil blade at a turbine rotational speed of 400 rpm of 57.05%, while for the lowest turbine efficiency found in the NACA-9405 R variation with a 200 rpm turbine rotational speed of 40.04%. This Efficiency result is relatively smaller than other studies' results [19][20][21]. However, this study is more efficient than another study that utilizes crossflow turbines without a nozzle [22].

3.2 Discussion of the water fraction contour

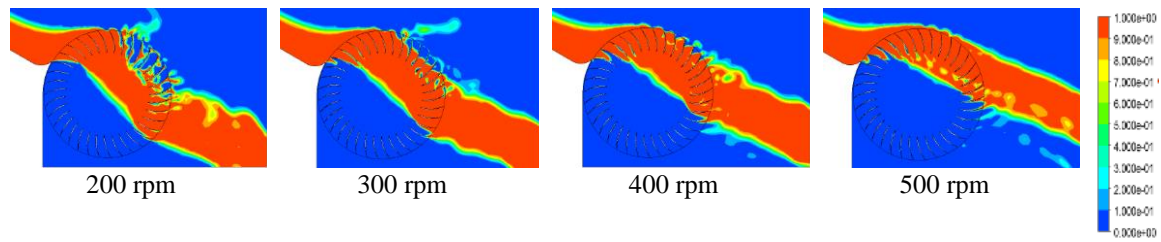
| 200 rpm | 300 rpm | 400 rpm | 500 rpm |

Figure 8. The contours of the rotation variation results

Based on Figure 8, it is found that for all variations in the shape of the airfoil blades, with a turbine rotational speed of 200 rpm and 300 rpm, the thickness of the water flow inside the turbine or when it exits from the upper blades enters the lower blades of the turbine is relatively small when compared to speed 400rpm. This phenomenon is because the thickness of the water flow that passes through the turbine at this speed has a thicker velocity, which is an advantage. Because the wider the water flow that rotates the turbine, the better energy conversion on the turbine blades is produced, so the force generated will also increase based on the energy conversion that occurs. However, if you look at the turbine's rotational speed of 500 rpm, even though it has a reasonably good thickness of water flow, it can be seen that there is a flow of water coming out of the top blades of the turbine, resulting in the energy of the water flow not being fully converted resulting in a smaller force. Compared to the turbine rotational speed of 400 rpm.

3.3 Simulation Validation

Validation is carried out to check whether the simulation results are close to valid or not close to correct by comparing the simulated data with theoretical or experimental data. This study uses the error validation method for the simulation validation process, and theoretical data is taken as comparative data, where the theoretical data is taken from the velocity triangle method for crossflow water turbines. The speed triangle method can be seen in Figure 9.
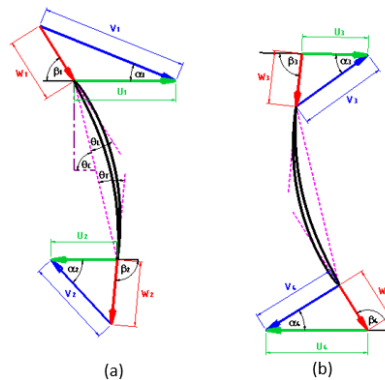

Figure 9 Airfoil blade velocity triangle (a) Upper blade (b) Lower blade

From these data and then processed using equations 4 to 14, the resulting efficiency for NACA-9405 blades is 58.96%, NACA-9503 is 59.25%, and NACA-9506 is 58.55%. So to produce an error value on efficiency, results can be calculated using the following equation 22.

$$Error = \frac{\eta_{Theoretic} - \eta_{Simulation}}{\eta_{Theoretic}} \cdot 100\% \tag{22}$$

Then the error value is generated, as shown in the table below

Table 5. Error calculation results

NACA	$\eta_{Theoretical}$ (%)	$\eta_{Simulation}$ (%)	Eror (%)
9405	58,07	56.82	2,15
9503	59,25	57.05	3,71
9506	58,55	54.78	6,44

Based on Table 5, using the equation above and the simulation data taken is the highest efficiency. The NACA-9405 airfoil, with a simulation efficiency of 56.82%, produces an error value of 2.15%. The NACA-

9503, with an efficiency of 57.05% based on the CFD result, creates an error value of 3.71%, and NACA-9506, with an efficiency of 54.78%, produces an error value of 6.44%. From the error validation calculations results from some of the data, it makes a value of less than 10%. Therefore, it can be concluded that the simulations carried out are close to valid.

4. CONCLUSIONS

The effect of applying the shape of the airfoil blade on the performance of an open-flow crossflow turbine has been simulated and compared. The result is that the NACA-9405 R blade has the highest power value of 3.74 kW. The highest efficiency is 52.89%, the NACA-9405 F blade produces the highest power of 4.02 kW with the highest efficiency of 56.82%, then on NACA-9503 R it obtains the most elevated power value of 3.95 kW and the highest efficiency of 55.78%, for NACA-9503 F it produces the highest power of 4.04 kW with the highest efficiency of 57.05%, this variation is a variation with delivers the highest data of all variations. In comparison, NACA-9506 R obtains the highest power of 3.80 kW with the highest efficiency of 53.72%, and finally, NACA-9506 F produces the highest power of 3.88 kW and the highest efficiency of 54.78 %. All variations that deliver the highest power and efficiency are obtained by varying the turbine rotational speed of 400 rpm.

REFERENCES

[1]   BPS-Statistics Indonesia, "Jumlah Desa Tertinggal," 2018. https://www.bps.go.id/indikator/indikator/view_data/0000/data/1231/sdgs_10/1 (accessed Sep. 22, 2022).

[2]   J. Vintarno, Y. S. Sugandi, and J. Adiwisastra, "Perkembangan penyuluhan pertanian dalam mendukung pertumbuhan pertanian di Indonesia," *Responsive: Jurnal Pemikiran Dan Penelitian Administrasi, Sosial, Humaniora Dan Kebijakan Publik*, vol. 1, no. 3, pp. 90–96, 2019.

[3]   B. Pranoto, S. N. Aini, H. Soekarno, A. Zukhrufiyati, H. Al Rasyid, and S. Lestari, "Potensi energi mikrohidro di daerah irigasi (studi kasus di wilayah sungai serayu opak)," *Jurnal Irigasi*, vol. 12, no. 2, pp. 77–86, 2018.

[4]   L. Ersado, *Small-scale irrigation dams, agricultural production, and health: theory and evidence from Ethiopia*, vol. 3494. World Bank Publications, 2005.

[5]   Y. A. Çengel and J. M. Cimbala, *Fluid Mechanics A Fundamental Approach*. 2018.

[6]   A. Indra Siswantara *et al.*, *Assessment of Turbulence Model for Crossflow Pico Hydro Turbine Numerical Simulation*, vol. 10, no. 2. Penerbit Akademia Baru, 2018.

[7]   Budiarso, D. Adanta, A. P. Prakoso, A. I. Siswantara, and R. Dianofitra, "Comparison between Airfoil NACA-6712 Profiled and Ordinary Blade in Crossflow Turbine by Numerical Simulation," in *15th International Conference on Quality in Research*, 2017. Accessed: Jan. 22, 2019. [Online]. Available: https://www.researchgate.net/publication/328012776

[8]   M. Gotoh, H. Kowata, T. Okuyama, and S. Katayama, "Damming-up Effect of a Current Water Wheel set in a Rectangular Channel," *World Renewable Energy Congress VI*, pp. 1615–1618, Jan. 2000, doi: 10.1016/B978-008043865-8/50333-0.

[9]   D. P. Sari *et al.*, "Performance of undershot waterwheel in pico scale with difference in the blades number," *Journal of the Brazilian Society of Mechanical Sciences and Engineering*, vol. 44, no. 3, p. 107, 2022, doi: 10.1007/s40430-022-03430-0.

[10]   A. P. A. P. Prakoso *et al.*, "Comparison Between 6-DOF UDF and Moving Mesh Approaches in CFD Methods for Predicting Crossflow Pico- Hydro Turbine Performance," *CFD Letters*, vol. 11, no. 6, pp. 86–96, 2019.

[11]   D. Adanta, D. P. Sari, N. M. Muhammad, and A. P. Prakoso, "HISTORY OF UTILIZATION OF THE COMPUTATIONAL FLUID DYNAMICS METHOD FOR STUDY PICO HYDRO TYPE CROSSFLOW," *Indonesian Journal of Engineering and Science (IJES)*, vol. 2, no. 1, pp. 17–24, 2021.

[12]   P. Breeze, *Hydropower*. Academic Press, 2018.

[13]   Ľ. Jurík, M. Zeleňáková, T. Kaletová, and A. Arifjanov, "Small water reservoirs: sources of water for irrigation," *Water Resources in Slovakia: Part I: Assessment and Development*, pp. 115–131, 2019.

[14]   R. Arvian, *ANALISIS PENGARUH KEMIRINGAN KANAL TERBUKA TERHADAP KINERJA TURBIN CROSS-FLOW ALIRAN TERBUKA SECARA NUMERIK*. Cimahi: Repository Skripsi Universitas Jenderal Achmad Yani, 2022.

[15]   D. Adanta *et al.*, "Performance comparison of NACA 6509 and 6712 on pico hydro type crossflow turbine by numerical method," *Journal of Advanced Research in Fluid Mechanics and Thermal Sciences*, vol. 45, no. 1, pp. 116–127, 2018, [Online]. Available: www.akademiabaru.com/arfmts.html

[16]   S. Himran, "Turbin Air; Teori & Dasar Perencanaan," 2018.

[17]   V. Sammartano, C. Aricò, A. Carravetta, O. Fecarotta, and T. Tucciarelli, "Banki-michell optimal design by computational fluid dynamics testing and hydrodynamic analysis," *Energies (Basel)*, vol. 6, no. 5, pp. 2362–2385, 2013.

[18]   S. H. A. N. E. A. RICHARDS, "Completed Richardson extrapolation in space and time," *Commun Numer Methods Eng*, vol. 13, no. 7, pp. 573–582, 1997.

[19]   V. Sammartano, G. Morreale, M. Sinagra, and T. Tucciarelli, "Numerical and experimental investigation of a crossflow water turbine," *Journal of Hydraulic Research*, vol. 54, no. 3, pp. 321–331, May 2016, doi: 10.1080/00221686.2016.1147500.

[20]   N. Acharya, C.-G. Kim, B. Thapa, and Y.-H. Lee, "Numerical analysis and performance enhancement of a crossflow hydro turbine," *Renew Energy*, vol. 80, pp. 819–826, 2015.

[21]   R. Adhikari and D. Wood, "The Design of High Efficiency Crossflow Hydro Turbines: A Review and Extension," *Energies (Basel)*, vol. 11, no. 2, p. 267, 2018.

[22]   A. H. Elbatran, O. B. Yaakob, Y. M. Ahmed, and A. S. Shehata, "Numerical and experimental investigations on efficient design and performance of hydrokinetic Banki cross flow turbine for rural areas," *Ocean Engineering*, vol. 159, no. December 2017, pp. 437–456, 2018, doi: 10.1016/j.oceaneng.2018.04.042.